

## JGR Biogeosciences

## RESEARCH ARTICLE

10.1029/2020JG005631

## Key Points:

- Ammonium oxidation is the dominant N<sub>2</sub>O production pathway in suboxic Saanich Inlet
- Addition of nitrate and nitrite stimulates N<sub>2</sub>O production in anoxic, N<sub>2</sub>O-depleted deep water
- Oxygenation of anoxic water enhances N<sub>2</sub>O production via ammonium oxidation and increases water column N<sub>2</sub>O supersaturation level

## Supporting Information:

- Supporting Information S1

## Correspondence to:

Q. Ji,  
jqixing@mail.sysu.edu.cn

## Citation:

Ji, Q., Jameson, B. D., Juniper, S. K., & Grundle, D. S. (2020). Temporal and vertical oxygen gradients modulate nitrous oxide production in a seasonally anoxic fjord: Saanich Inlet, British Columbia. *Journal of Geophysical Research: Biogeosciences*, 125, e2020JG005631. <https://doi.org/10.1029/2020JG005631>

Received 5 JAN 2020

Accepted 25 JUL 2020

Accepted article online 28 AUG 2020

## Author Contributions:

**Conceptualization:** Qixing Ji, Damian S. Grundle

**Formal analysis:** Qixing Ji

**Funding acquisition:** Damian S. Grundle

**Investigation:** Qixing Ji, Brett D. Jameson, Damian S. Grundle

**Methodology:** Qixing Ji, S. Kim Juniper, Damian S. Grundle

**Supervision:** Damian S. Grundle

**Visualization:** Qixing Ji

**Writing - original draft:** Qixing Ji, Brett D. Jameson, S. Kim Juniper, Damian S. Grundle

**Writing - review & editing:** Qixing Ji, Brett D. Jameson, S. Kim Juniper, Damian S. Grundle

## Temporal and Vertical Oxygen Gradients Modulate Nitrous Oxide Production in a Seasonally Anoxic Fjord: Saanich Inlet, British Columbia

Qixing Ji<sup>1,2,3</sup> , Brett D. Jameson<sup>4</sup> , S. Kim Juniper<sup>4,5,6</sup>, and Damian S. Grundle<sup>3</sup>

<sup>1</sup>School of Marine Sciences, Sun Yat-Sen University, Zhuhai, China, <sup>2</sup>GEOMAR, Helmholtz Centre for Ocean Research Kiel, Kiel, Germany, <sup>3</sup>Bermuda Institute of Ocean Sciences, St. George's, Bermuda, <sup>4</sup>School of Earth and Ocean Sciences, Bob Wright Centre, University of Victoria, Victoria, British Columbia, Canada, <sup>5</sup>Department of Biology, University of Victoria, Victoria, British Columbia, Canada, <sup>6</sup>Ocean Networks Canada, Victoria, British Columbia, Canada

**Abstract** Nitrous oxide (N<sub>2</sub>O) is a strong greenhouse gas and an ozone depleting agent. In marine environments, N<sub>2</sub>O is produced biologically via ammonium oxidation, nitrite, and nitrate reduction. The relative importance of these principle production pathways is strongly influenced by oxygen availability. We conducted <sup>15</sup>N tracer experiments of N<sub>2</sub>O production in parallel with measurements of N<sub>2</sub>O concentration and natural abundance isotopes/isotopomers in Saanich Inlet, a seasonally anoxic fjord, to investigate how temporal and vertical oxygen gradients regulate N<sub>2</sub>O production pathways and rates. In April, June, and August 2018, the depth of the oxic-anoxic interface (dissolved oxygen = 2.5 μmol L<sup>-1</sup> isoline) progressively deepened from 110 to 160 m. Within the oxygenated and suboxic water column, N<sub>2</sub>O supersaturation coincided with peak ammonium oxidation activity. Conditions in the anoxic deep water were potentially favorable to N<sub>2</sub>O production from nitrate and nitrite reduction, but N<sub>2</sub>O undersaturation was observed indicating that N<sub>2</sub>O consumption exceeded rates of production. In October, tidal mixing introduced oxygenated water from outside the inlet, displacing the suboxic and anoxic deep water. This oxygenation event stimulated N<sub>2</sub>O production from ammonium oxidation and increased water column N<sub>2</sub>O supersaturation while inhibiting nitrate and nitrite reduction to N<sub>2</sub>O. Results from <sup>15</sup>N tracer incubation experiments and natural abundance isotopomer measurements both implicated ammonium oxidation as the dominant N<sub>2</sub>O production pathway in Saanich Inlet, fueled by high ammonium fluxes (0.6–3.5 nmol m<sup>-2</sup> s<sup>-1</sup>) from the anoxic depths. Partial denitrification contributed little to water column N<sub>2</sub>O production because of low availability of nitrate and nitrite.

### 1. Introduction

Nitrous oxide (N<sub>2</sub>O) is an important atmospheric trace gas that regulates Earth's climate through catalysis of stratospheric ozone depletion (Crutzen, 1970) and absorption of long wave radiation (Yung et al., 1976). Globally, N<sub>2</sub>O is mostly produced by biological activities (Codispoti, 2010), such that understanding the N<sub>2</sub>O cycling pathways and associated regulating factors is a prerequisite for N<sub>2</sub>O budget estimates, particularly in the marine environment (Bange et al., 2019; Wilson et al., 2018). The biological production of N<sub>2</sub>O is attributed to nitrogen cycling processes, during which N<sub>2</sub>O can be produced as a by-product of aerobic oxidation of ammonium (NH<sub>4</sub><sup>+</sup>) to nitrite (i.e., the first step of nitrification) and as an important intermediate during the anaerobic reduction of nitrate (NO<sub>3</sub><sup>-</sup>) and nitrite (NO<sub>2</sub><sup>-</sup>). Consumption of N<sub>2</sub>O occurs under anoxic conditions where heterotrophic bacteria reduce N<sub>2</sub>O to N<sub>2</sub>. Over 40% of natural N<sub>2</sub>O emissions occur in marine and freshwater environments (Ciais et al., 2013). Notably, high N<sub>2</sub>O emissions are often associated with steep vertical oxygen gradients (oxyclines), such as those found in open ocean oxygen minimum zones (OMZs) with nanomolar oxygen at intermediate depths, and eutrophic coastal waters (Bange et al., 1996; Buitenhuis et al., 2018). While open ocean N<sub>2</sub>O emission estimates are relatively well constrained (Buitenhuis et al., 2018), coastal emissions are highly uncertain (Maavara et al., 2019), primarily due to highly variable spatial and temporal gradients of dissolved oxygen concentration (DO) and organic matter export (de Bie et al., 2002; Laperriere et al., 2019). Projecting future N<sub>2</sub>O emission scenarios requires a better understanding of the spatial and temporal dynamics of N<sub>2</sub>O production in relation to environmental variability, especially in productive coastal environments.

Saanich Inlet, a well-studied seasonally anoxic fjord, was chosen as the experimental site to investigate how temporal and vertical variability of dissolved oxygen regulates  $N_2O$  production in coastal waters. Located on southern Vancouver Island in British Columbia, Canada, Saanich Inlet has a central deep basin (~215 m) and a shallow sill (~70 m) at its north facing mouth, which restricts deepwater movement in and out of the fjord (Herlinveaux, 1962). Spring-neap tidal mixing at the seaward end of the fjord introduces new nutrients (primarily  $NO_3^-$ ) to the surface waters of Saanich Inlet on a fortnightly basis (Gargett et al., 2003), resulting in high new primary production (Grundle & Juniper, 2011; Grundle et al., 2009). Rapid sinking of particulate organic matter and subsequent remineralization cause water column deoxygenation (Timothy & Soon, 2001), creating a steep oxycline on top of the anoxic bottom water where hydrogen sulfide ( $H_2S$ ) accumulates (Cohen, 1978; Torres-Beltrán et al., 2017). Deepwater oxygen renewal events occur primarily in later summer and fall, when dense oxygenated water accumulates outside of the fjord and periodically flows over the sill and into the basin (Anderson & Devol, 1973; Manning et al., 2010). These features make Saanich Inlet an ideal natural laboratory to examine the effects of dissolved oxygen availability on nitrogen cycling (Bourbonnais et al., 2013; Grundle & Juniper, 2011; Ward & Kilpatrick, 1990), greenhouse gas fluxes (Capelle et al., 2018, 2019), and microbial community dynamics (Torres-Beltrán et al., 2016; Zaikova et al., 2010). The detailed biogeochemical characterizations of Saanich Inlet provide a foundation for further exploration of  $N_2O$  production pathways and the regulating environmental factors, which have not been reported. In this study, we have built upon earlier nitrogen cycling studies by conducting  $^{15}N$  tracer incubation experiments to directly measure  $N_2O$  production via multiple pathways along vertical and temporal oxygen gradients. The analyses of natural abundance bulk  $N_2O$  isotopes ( $^{15}N$  versus  $^{14}N$  and  $^{18}O$  versus  $^{16}O$ ) and isotopomers (the intramolecular configuration of nitrogen isotopes within the linear  $N_2O$  molecule) provide a further indication of how the different metabolic pathways have contributed to total  $N_2O$  production in Saanich Inlet. For example,  $^{15}N$  tracer experiments determine potential and instantaneous  $N_2O$  production rates and pathways (Ji et al., 2018), whereas  $N_2O$  isotopomeric measurements reveal the dominant  $N_2O$  production pathway integrated over the history of a water mass (Fujii et al., 2013). The isotope measurements reported here were conducted on a recently developed laser-based analytical system that is able to deliver accuracy and precision comparable to traditional isotope ratio mass spectrometer techniques (Ji & Grundle, 2019). This work combines  $^{15}N$  tracer incubation,  $N_2O$  concentration, and natural abundance isotopic/isotopomeric measurements to (1) elucidate the  $N_2O$  dynamics in a model coastal marine system with temporal and vertical oxygen gradients, (2) examine oxygen regulation of  $N_2O$  production pathways during bottle incubations and under in situ conditions, and (3) identify the major  $N_2O$  production pathways potentially contributing to atmospheric emissions.

## 2. Materials and Methods

### 2.1. Field Sampling

Four cruises were conducted on the *MSV John Strickland* in 2018 to conduct sampling in Saanich Inlet. Our sampling site ( $48^{\circ}38.58'N$ ,  $123^{\circ}29.93'W$ , depth 206 m, Figure S1) was ~10 km south of the inlet's mouth and ~5 km north of the monthly  $N_2O$  time series station reported by Capelle et al. (2018). Bimonthly sampling was conducted on 5 April, 14 June, 2 August, and 25 October 2018 to represent the transition from stable water column stratification and bottom water anoxia to deepwater oxygen renewal.

Six discrete sampling depths below the euphotic zone (75, 90, 100, 110, 130, and 160 m) were chosen to bracket the oxycline and were maintained consistently throughout the four cruises. Water samples were collected from 5-L Niskin bottles on a rosette sampler equipped with a conductivity-temperature-depth (CTD) package (SBE 19, Sea-Bird Electronics, Bellevue, WA). The CTD rosette was also equipped with an oxygen sensor (SBE 43, Sea-Bird Electronics) for real time, continuous profiling of DOs. Dissolved oxygen was also measured in discrete samples, using the Carpenter-Winkler titration method (Carpenter, 1965) for the purpose of calibrating the oxygen sensor. The discrete DO measurements generally had a reproducibility of 2% of mean values, and the oxygen sensor had a detection limit of  $\sim 2.5 \mu\text{mol L}^{-1}$ . We operationally define the terms *anoxic* as DO ranging from 0 to  $2.5 \mu\text{mol L}^{-1}$ , *suboxic* as 2.5 to  $15 \mu\text{mol L}^{-1}$ , and *oxygenated* as greater  $15 \mu\text{mol L}^{-1}$ . It should be noted that at anoxic conditions ( $DO = 0\text{--}2.5 \mu\text{mol L}^{-1}$ ), denitrification and sulfate reduction are probably the dominant microbial metabolism, yet oxygen respiration continues to operate even at nanomolar DO level (Zakem & Follows, 2017). And thus, denitrification, sulfate reduction and

oxygen respiration coexist at suboxic depths in Saanich Inlet (Bourbonnais et al., 2013; Manning et al., 2010; Torres-Beltrán et al., 2016). Seawater subsamples for nutrient measurements were filtered (0.22- $\mu\text{m}$  Sterivex™ filter, EMD Millipore, Burlington, MA) and stored at  $-20\text{ }^{\circ}\text{C}$  in acid-washed 60-ml high-density polyethylene bottles (20,160,060, Thermo Scientific, Waltham, MA, USA).

Duplicate samples for  $\text{N}_2\text{O}$  concentration measurements were filled from 5-L Niskin bottles into the bottom of 20-ml glass serum vials (LPP.10732, LEAP PAL Parts, Raleigh, NC, United States) and then were allowed to overflow at least three times the volume before sealing the vials with butyl septa (60180744, Thermo Scientific) and aluminum rings (60180512, Thermo Scientific). The mean volume of a crimp-sealed vial was  $20.3 \pm 0.06$  ml. Duplicate samples for  $\text{N}_2\text{O}$  isotope and isotopomer measurements were crimp sealed in 60-ml glass serum bottles (223745, Wheaton, Millville, New Jersey, United States). Both concentration and isotope/isotopomer samples were immediately preserved with 0.05 ml of saturated mercuric chloride solution ( $\text{HgCl}_2$ ). Samples were stored in the dark at 20 to 23  $^{\circ}\text{C}$  for less than 4 months before laboratory analyses (described in section 2.3).

## 2.2. Nitrogen Tracer Experiments

For  $\text{N}_2\text{O}$  production experiments, seawater was sampled from 5-L Niskin bottles into crimp-sealed 20-ml vials using the same technique as described for the  $\text{N}_2\text{O}$  concentration samples. To facilitate tracer addition, a 1-ml  $\text{N}_2$  headspace was created in the crimp-sealed vials. During the October sampling, the four shallower depths (75, 90, 100, and 110 m) were treated with an air headspace to maintain oxygenated conditions. Final DOs in the water phase were calculated using equilibrium concentrations between the water and gas phases in the incubation vials (Garcia & Gordon, 1992) and were later confirmed by laboratory oxygen sensor measurements in a similar experimental setup (see supporting information Text S1). The water phase DO in vials with an  $\text{N}_2$  headspace was approximately 40% of in situ concentration, whereas air headspace vials had elevated DO ranging from 187 to 210  $\mu\text{mol L}^{-1}$ , in comparison to in situ DO of 43–101  $\mu\text{mol L}^{-1}$  (see supporting information Table S1 for DO of all incubation experiments). Incubation experiments with  $^{15}\text{N}$  tracers were applied to quantify rates of  $\text{N}_2\text{O}$  production from  $\text{NH}_4^+$  oxidation,  $\text{NO}_2^-$ , and  $\text{NO}_3^-$  reduction. Three suites of  $^{15}\text{N}$  tracer solutions ( $^{15}\text{NH}_4^+$  plus  $^{14}\text{NO}_2^-$ ,  $^{15}\text{NO}_2^-$  plus  $^{14}\text{NH}_4^+$ ,  $^{15}\text{NO}_3^-$  plus  $^{14}\text{NH}_4^+$ , and  $^{14}\text{NO}_2^-$ , Sigma-Aldrich, St. Louis, Missouri, United States) were applied to enrich  $^{15}\text{NH}_4^+$ ,  $^{15}\text{NO}_2^-$ , and  $^{15}\text{NO}_3^-$  to 0.5, 0.5 and 1.0  $\mu\text{mol L}^{-1}$  (final concentration, tracer  $^{15}\text{N}$  atom % = 99%), respectively, and increased concentrations of  $^{14}\text{NH}_4^+$ ,  $^{14}\text{NO}_2^-$ , or  $^{14}\text{NO}_3^-$  by 0.5, 0.5, and 1.0  $\mu\text{mol L}^{-1}$ , respectively. Tracers were dissolved in deionized water, and the solutions were flushed with  $\text{N}_2$  before adding 0.1 ml into each vial. The set of incubations with  $^{15}\text{NH}_4^+$  plus  $^{14}\text{NO}_2^-$  was also used for measuring nitrification rates (oxidation of  $\text{NH}_4^+$  to  $\text{NO}_2^-$  and  $\text{NO}_3^-$ ), which allowed us to estimate the yield of  $\text{N}_2\text{O}$  from nitrification, defined as the molar nitrogen ratio of  $\text{N}_2\text{O}$  production to  $\text{NH}_4^+$  oxidation (see section 3.4). Incubations lasted 12 to 18 hr in temperature-controlled chambers ( $\pm 1\text{ }^{\circ}\text{C}$  of in situ temperature), during which duplicate samples were preserved every 6 to 9 hr (3 time points in total) with 0.05 ml of saturated  $\text{HgCl}_2$  solution. Preserved samples were stored in the dark at 20 to 23  $^{\circ}\text{C}$  for less than 4 months before performing  $\text{N}_2\text{O}$  isotopic/isotopomeric analyses (see section 2.3).

## 2.3. Laboratory Analyses

Concentrations of dissolved inorganic nitrogen species ( $\text{NH}_4^+$ ,  $\text{NO}_2^-$  and  $\text{NO}_3^-$ ) were determined as follows:  $\text{NH}_4^+$  was measured fluorometrically by reaction with orthophthaldialdehyde (Holmes et al., 1999), with a detection limit of 0.02  $\mu\text{mol L}^{-1}$ ;  $\text{NO}_2^-$  was treated with the Griess reagent and measured colorimetrically (Hansen & Koroleff, 1999), with a detection limit of 0.005  $\mu\text{mol L}^{-1}$  (using a 10-cm cuvette); and  $\text{NO}_3^- + \text{NO}_2^-$  was measured using the cadmium reduction method (Hansen & Koroleff, 1999), with a detection limit of 0.02  $\mu\text{mol L}^{-1}$ . Although not experimentally measured, the presence of hydrogen sulfide ( $\text{H}_2\text{S}$ ) was indicated by its recognizable smell. However, samples for nutrient analyses were filtered in open air, and  $\text{H}_2\text{S}$  was probably oxidized. It is therefore unlikely for  $\text{H}_2\text{S}$  to have interfered with  $\text{NO}_3^- + \text{NO}_2^-$  measurements.

Analyses of  $\text{N}_2\text{O}$  concentration and isotope/isotopomer ratios were performed using a purge-and-trap module coupled to a cavity ring-down spectrometer (PT-CRDS) recently developed in the Grundle Laboratory. The PT-CRDS is an automated, laser-based system that provides comparable accuracy and precision to gas chromatography and isotope ratio mass spectrometer techniques for  $\text{N}_2\text{O}$  concentration and

isotope/isotopomer ratio measurements, respectively. A full description of this technique is outlined in Ji and Grundle (2019). Isotopic analysis determines the relative abundances of nitrogen isotopes ( $\delta^{15}\text{N}_{\text{bulk}}$ ) and oxygen isotopes ( $\delta^{18}\text{O}$ ) of the entire  $\text{N}_2\text{O}$  pool, whereas isotopomeric analysis discerns the intramolecular nitrogen isotope substitution (isotopomers) on the linear asymmetric  $\text{N}_2\text{O}$  molecule ( $\text{N} = \text{N} = \text{O}$ ). By convention, the relative abundance of  $^{15}\text{N}$  substitutions of the central ( $^{14}\text{N} = ^{15}\text{N} = ^{16}\text{O}$ ) and terminal positions ( $^{15}\text{N} = ^{14}\text{N} = ^{16}\text{O}$ ) are denoted as  $\delta^{15}\text{N}_2\text{O}_\alpha$  and  $\delta^{15}\text{N}_2\text{O}_\beta$ , respectively. Briefly, the PT-CRDS analyses employed the following methodology: Dissolved  $\text{N}_2\text{O}$  in sample vials was extracted by  $\text{N}_2$  purging and cryo-trapped using liquid nitrogen at working temperature of  $130 \pm 10$  K (note that  $\text{N}_2\text{O}$  boiling temperature is 185 K). Heating to 480 K released the gaseous  $\text{N}_2\text{O}$ , after which concentrations and isotope/isotopomer ratios were measured by quantitative light dissipation at specific wavelengths ( $^{14}\text{N} = ^{15}\text{N} = ^{16}\text{O}$ ,  $^{15}\text{N} = ^{14}\text{N} = ^{16}\text{O}$ , and  $^{14}\text{N} = ^{14}\text{N} = ^{18}\text{O}$  at 2195.76195, 2198.79576, and 2195.95102  $\text{cm}^{-1}$ , respectively). Raw isotopic measurements were corrected for sample size-dependent isotopic deviations caused by varying  $\text{N}_2\text{O}$  concentrations (Ji & Grundle, 2019) and calibrated with isotopic reference materials (see Table S2). Because the optimal quantity of  $\text{N}_2\text{O}$  for highly accurate isotopic/isotopomeric analyses by PT-CRDS is 0.5–0.8 nmol- $\text{N}_2\text{O}$ , samples from 130 and 160 m in April and 160 m samples in June did not contain enough  $\text{N}_2\text{O}$ , and, as such, those results are not reported.

The  $^{15}\text{NH}_4^+$  incubation set was used for quantifying nitrification rates after measuring  $\delta^{15}\text{N}\text{-N}_2\text{O}$ . Nitrification rates were determined as the transfer of nitrogen from  $\text{NH}_4^+$  to  $\text{NO}_2^- + \text{NO}_3^-$  (Laperriere et al., 2019). The  $\delta^{15}\text{N}$  signature of  $\text{NO}_2^- + \text{NO}_3^-$  ( $\delta^{15}_{\text{NO}_x^-}$ ) was measured using the same PT-CRDS technique outlined above, but only after first converting the  $\text{NO}_2^- + \text{NO}_3^-$  to  $\text{N}_2\text{O}$  in crimp-sealed 20-ml vials using the denitrifier method (Weigand et al., 2016). A set of 20-ml vials (LPP.10732, LEAP PAL Parts, Raleigh, NC, United States) containing live bacterial concentrate *Pseudomonas chlororaphis* (ATCC® 43928™, Manassas, Virginia) in buffer solution (pH = ~7.3) were purged with nitrogen gas to create anaerobic conditions in the vials. The water samples were treated with 0.05 ml of 10 mol  $\text{L}^{-1}$  sodium hydroxide solution in order to precipitate mercury; the supernatant was transferred to the bacterial vials for complete conversion of  $\text{NO}_2^- + \text{NO}_3^-$  to  $\text{N}_2\text{O}$  within 3 hr of incubation at 22 °C. As the  $\text{NO}_2^- + \text{NO}_3^-$  concentrations of water samples ranged from 0.6 to 32  $\mu\text{mol L}^{-1}$ , the volume of water sample injected for bacterial conversion was adjusted to accommodate 0.5 nmol- $\text{N}_2\text{O}$  in order to achieve accurate  $\delta^{15}\text{N}$  measurements by the PT-CRDS. To calibrate the measurements, isotopic reference vials were prepared by bacterial conversion of potassium nitrate USGS-35 ( $\delta^{15}\text{N} = 2.7\%$  versus Air  $\text{N}_2$ ) and USGS-32 ( $\delta^{15}\text{N} = 180\%$  versus Air  $\text{N}_2$ ).

#### 2.4. Data Processing

Water column  $\text{N}_2\text{O}$  saturation was quantified by the  $\text{N}_2\text{O}$  excess ( $\Delta\text{N}_2\text{O}$ ), defined as the concentration difference between measured and equilibrium values with respect to the atmosphere.

$$\Delta\text{N}_2\text{O} = [\text{N}_2\text{O}]_{\text{measured}} - [\text{N}_2\text{O}]_{\text{equilibrium}} \quad (1)$$

Equilibrium  $\text{N}_2\text{O}$  concentrations are temperature and salinity dependent and were calculated according to Weiss and Price (1980) using atmospheric  $\text{N}_2\text{O}$  concentration of 330 ppb.

The  $\delta$  notation is used to quantify the relative abundance of  $\text{N}_2\text{O}$  isotopomers (Coplen, 2011) in Equations 2 and 3.

$$\delta^{15}\text{N}_2\text{O}_\alpha = \frac{(^{14}\text{N}^{15}\text{N}^{16}\text{O}/^{14}\text{N}^{14}\text{N}^{16}\text{O})}{R_{\text{ref}}} - 1, \quad R_{\text{ref}} = \frac{^{15}\text{N}}{^{14}\text{N}} \text{ of atmospheric } \text{N}_2, \quad 0.003667 \quad (2)$$

$$\delta^{15}\text{N}_2\text{O}_\beta = \frac{(^{15}\text{N}^{14}\text{N}^{16}\text{O}/^{14}\text{N}^{14}\text{N}^{16}\text{O})}{R_{\text{ref}}} - 1, \quad R_{\text{ref}} = \frac{^{15}\text{N}}{^{14}\text{N}} \text{ of atmospheric } \text{N}_2, \quad 0.003667 \quad (3)$$

The bulk isotopes of  $\text{N}_2\text{O}$  are defined in Equations 4 and 5.

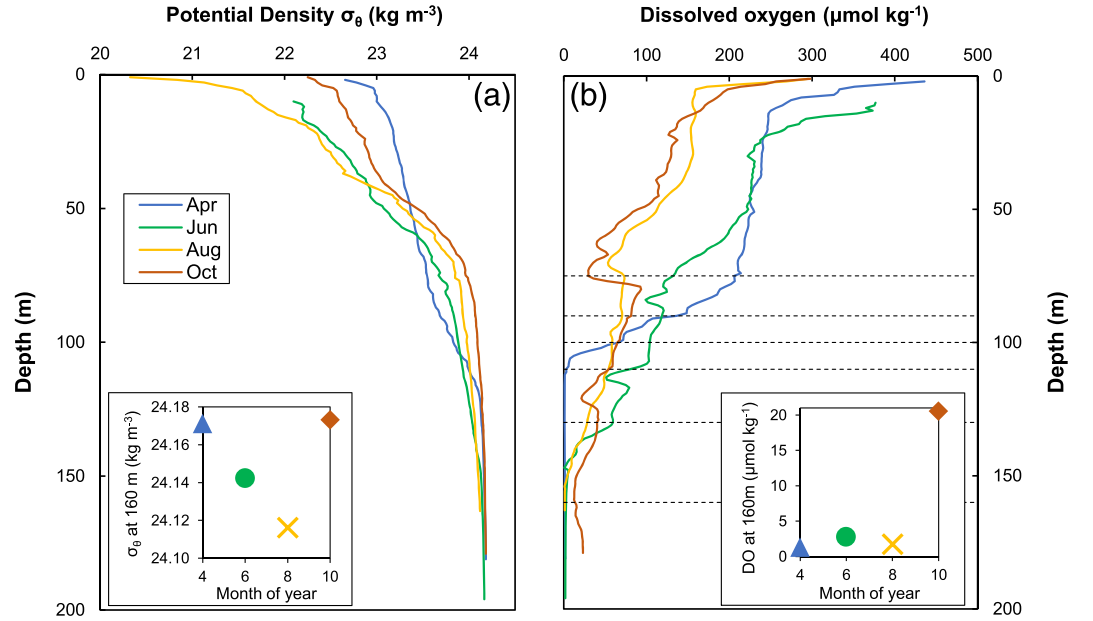


**Figure 1.** Profiles of water column (a) potential density and (b) dissolved oxygen at the sampling station in Saanich Inlet ( $48^{\circ}47.707'N$ ,  $123^{\circ}29.927'W$ ) during four campaigns in 2018 (April, June, August, and October). Inset figures of (a) and (b) show the potential density and dissolved oxygen at 160 m. Dashed lines in (b) indicate the sampling depths (75, 90, 100, 110, 130, and 160 m) for inorganic nitrogen analyses and  $N_2O$  production experiments.

$$\delta^{18}O-N_2O = \frac{(^{18}O/^{16}O)}{R_{ref}} - 1, \quad R_{ref} = \frac{^{18}O}{^{16}O} \text{ of VSMOW, } 0.002005 \quad (4)$$

$$\delta^{15}N_{bulk-N_2O} = \frac{\delta^{15}N_{\alpha} + \delta^{15}N_{\beta}}{2} \quad (5)$$

Site preference (SP) quantifies the relative abundance of the two  $N_2O$  isotopomers according to Equation 6.

$$SP = \delta^{15}N_{\alpha} - \delta^{15}N_{\beta} \quad (6)$$

The  $N_2O$  production rate  $R_{N_2O}$  ( $nmol-N L^{-1} day^{-1}$ ) is calculated according to Equation 7

$$R_{N_2O} = 2 \times \frac{d(^{15}N_2O)/dt}{F} \quad (7)$$

where  $^{15}N_2O$  represents concentration of  $^{15}N$ -labeled  $N_2O$  molecules,  $d^{15}N_2O/dt$  represents the slope of the linear regression of  $^{15}N_2O$  against time, and  $F$  represents  $^{15}N$  enrichment of substrate (2–99% at different depths). The conversion of  $\delta^{15}N_{bulk-N_2O}$  to  $^{15}N_2O$  is calculated according to Equation 8

$$^{15}N_2O = [N_2O] \times \frac{(\delta^{15}N_{bulk-N_2O} + 1) \times R_{ref}}{1 + (\delta^{15}N_{bulk-N_2O} + 1) \times R_{ref}} \quad (8)$$

where  $[N_2O]$  is the concentration of  $N_2O$  during the incubation experiments and  $R_{ref} = 0.003667$ . The detection limit of rate measurement was  $0.002 nmol-N L^{-1} day^{-1}$ .

Calculation of nitrification rate  $R_{nit}$  is according to Laperriere et al. (2019)

$$R_{nit} = \frac{d(^{15}NO_x^-)/dt}{F_{NH_4^+}^{15}} \quad (9)$$

where  $d^{15}NO_x^-/dt$  represents the slope of linear regression of  $^{15}N$  atom % of  $NO_3^- + NO_2^-$  (abbreviated as

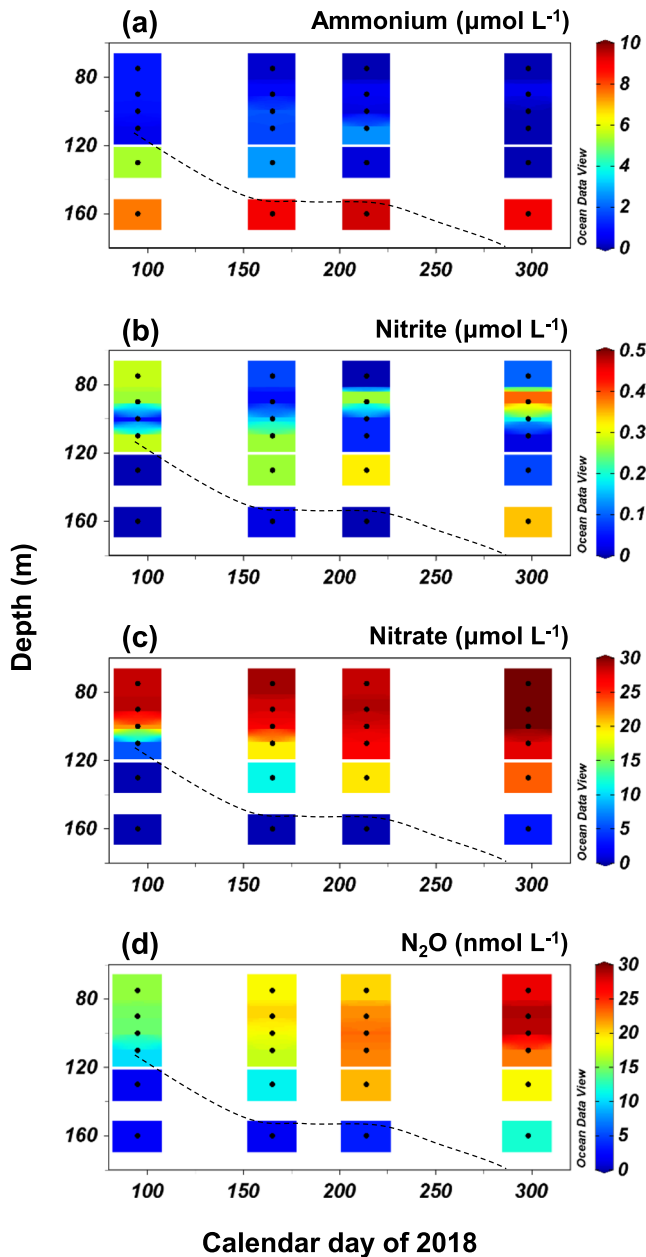


**Figure 2.** Concentration profiles of (a) ammonium, (b) nitrite, (c) nitrate, and (d) nitrous oxide at the sampling station (48°47.707'N, 123°29.927'W) during four sampling campaigns. Dashed line marks the approximate position of the oxic-anoxic interface (dissolved oxygen concentration =  $2.5 \mu\text{mol L}^{-1}$  isoline).

iated the anoxic conditions at these depths. In October, the entire water column was oxygenated ( $\text{DO} > 20 \mu\text{mol L}^{-1}$ , Figure 1b), indicating the progressive deepening of oxic-anoxic interface ( $\text{DO} = 2.5 \mu\text{mol L}^{-1}$  isoline) from April to October. Based on data from Ocean Networks Canada sensor platforms in Saanich Inlet (data not shown), oxygen renewal events appeared to have occurred in late August and mid-October. During these renewal events, dense and oxygenated water replaced the deep water inside the basin, increasing density and DO at 160 m (Figures 1a and 1b).

Inorganic nitrogen species ( $\text{NH}_4^+$ ,  $\text{NO}_2^-$ , and  $\text{NO}_3^-$ ) distributed differently along the oxycline. In shallower oxygenated waters,  $\text{NH}_4^+$  concentrations were generally  $\sim 1.0 \mu\text{mol L}^{-1}$ . Higher  $\text{NH}_4^+$  concentrations (5–

$\text{NO}_x^-$ ) on time and  $F_{\text{NH}_4^+}^{15\text{N}}$  represents  $^{15}\text{N}$  fraction labeled of substrate ammonium (5–99%). The value of  $^{15}\text{NO}_x^-$  is calculated according to Equation 10

$$^{15}\text{NO}_x^- = [\text{NO}_x^-] \times \frac{\left(\frac{\delta_{\text{NO}_x^-}^{15}}{1000} + 1\right) \times R_{\text{ref}}}{1 + \left(\frac{\delta_{\text{NO}_x^-}^{15}}{1000} + 1\right) \times R_{\text{ref}}} \quad (10)$$

where  $[\text{NO}_x^-]$  is the concentration of  $\text{NO}_3^- + \text{NO}_2^-$  during the incubation experiments and  $\delta_{\text{NO}_x^-}^{15}$  is the  $\delta^{15}\text{N}$  signature of  $\text{NO}_x^-$  measured by denitrifier method.

The nitrification  $\text{N}_2\text{O}$  yield is defined as the molar nitrogen ratio of  $\text{N}_2\text{O}$  versus nitrification. Two independent estimates of the  $\text{N}_2\text{O}$  yield are presented. First is the *rate ratio yield*, which is the ratio of directly measured rates of  $\text{N}_2\text{O}$  production versus nitrification during  $^{15}\text{NH}_4^+$  incubations, and it reveals instantaneous yield from bottle incubations at a range of oxygen levels. Note that oxygen concentrations in the incubation vials were different from those in situ levels (see section 2.2). Second is the *regression yield* using the nitrate- $\Delta\text{N}_2\text{O}$  relationship, which is based on by-production of  $\text{N}_2\text{O}$  during  $\text{NH}_4^+$  oxidation to  $\text{NO}_3^-$  in oxygenated waters below the euphotic zone, assuming stoichiometric conversion (i.e., 1 mol  $\text{NH}_4^+$ :1 mol  $\text{NO}_3^-$ ) and negligible accumulation of  $\text{NO}_2^-$  (Grundle et al., 2012; Rees et al., 2011). Such an indirect estimate reveals temporal- and spatial-averaged  $\text{N}_2\text{O}$  yield inside Saanich Inlet. To accurately characterize nitrate- $\Delta\text{N}_2\text{O}$  relationship during remineralization inside Saanich Inlet, we used  $\text{NO}_3^-$  and  $\Delta\text{N}_2\text{O}$  measurements from this study and a 9-year time series data set at 40–150 m depth from a nearby station in Saanich Inlet (Torres-Beltrán et al., 2017).

### 3. Results

#### 3.1. Water Column Structure and Chemistry

The water column potential density in Saanich Inlet ranged from 20.2 to 24.2  $\text{kg m}^{-3}$ . From April to August, a progressive decrease in density of the upper 50 m signaled increased stratification. The October water column had increased density in comparison to August. At 160 m, the density level of October was similar to that of April (Figure 1a). The DOs in the upper 10 m were high and often supersaturated (up to 140%). From April to August, in situ DO decreased with depth, with anoxic conditions persisting below 110 m in April and below 150 m in June and August (Figure 1b). The 160-m water samples from April, June, and August as well as 130 m from April exhibited recognizable  $\text{H}_2\text{S}$  odor, thus providing anecdotal evidence of its presence ( $\text{H}_2\text{S}$  was not measured here), and substantiated the anoxic conditions at these depths.

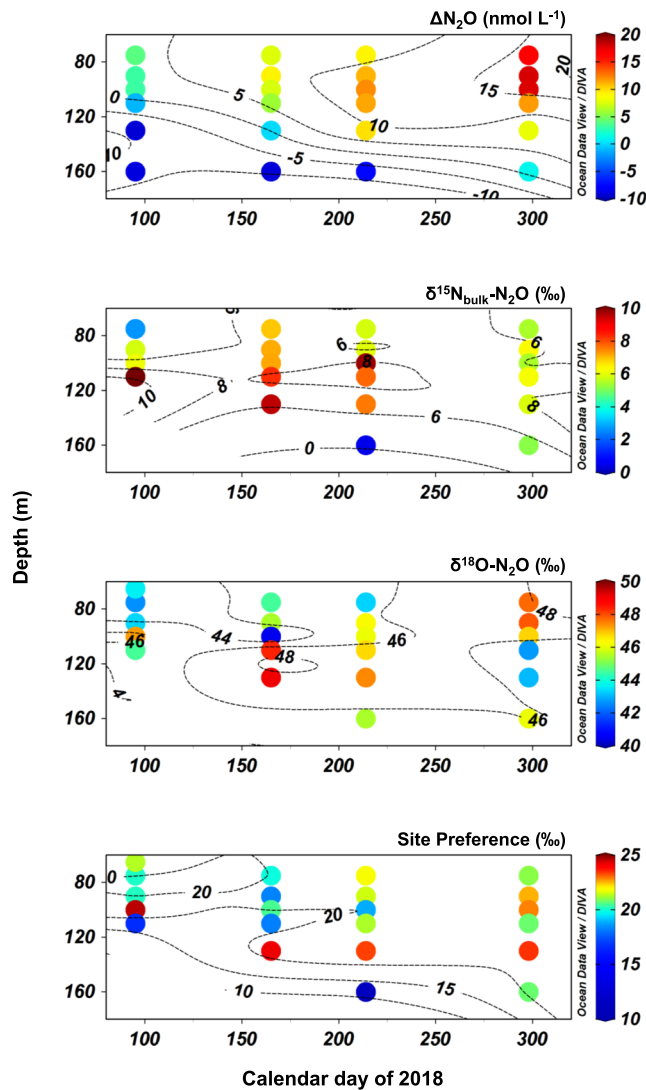


**Figure 3.** Water column profiles of (a)  $\text{N}_2\text{O}$  supersaturation ( $\Delta\text{N}_2\text{O}$ ), (b)  $\delta^{15}\text{N}_{\text{bulk-N}_2\text{O}}$ , (c)  $\delta^{18}\text{O-N}_2\text{O}$ , and (d) site preference at the sampling station. Contour lines were extrapolated using DIVA algorithm from Ocean Data View software.

$\text{N L}^{-1} \text{ day}^{-1}$ ). No production of  $\text{N}_2\text{O}$  from  $\text{NH}_4^+$  oxidation was detected at 130 m and below in April and at 160 m in June. In August,  $\text{NH}_4^+$  oxidation to  $\text{N}_2\text{O}$  was detected at 160 m despite anoxic conditions (Figure 4c). In October following the renewal event, all sampling depths showed  $\text{N}_2\text{O}$  production from  $\text{NH}_4^+$  oxidation, and the rates increased with depth. At 160 m where in situ DO was  $21 \mu\text{mol L}^{-1}$ , a maximum rate of  $\text{N}_2\text{O}$  production from  $\text{NH}_4^+$  oxidation was reached at  $\sim 1 \text{ nmol-N L}^{-1} \text{ day}^{-1}$  (Figure 4d), 3 to 25 times the maximum rates in April, June, and August.

Production of  $\text{N}_2\text{O}$  from  $\text{NO}_2^-$  reduction and  $\text{NO}_3^-$  reduction occurred at suboxic and anoxic conditions. Highest rates of  $\text{N}_2\text{O}$  production from  $\text{NO}_2^-$  reduction and  $\text{NO}_3^-$  reduction occurred at the oxic-anoxic interface, at 110 m in April (Figure 4e) and at 160 m in June and August (Figures 4f and 4g). These depths had pronounced  $\text{N}_2\text{O}$  undersaturation (Figure 3a) and low  $\text{NO}_2^-$  and  $\text{NO}_3^-$  concentrations that were close to the detection limit (Figures 2b and 2c). In October, low rates of  $\text{N}_2\text{O}$  production from  $\text{NO}_2^-$  and  $\text{NO}_3^-$  reduction were detected ( $< 0.09 \text{ nmol-N L}^{-1} \text{ day}^{-1}$ , Figure 4h); these rates generally increased with depth and with decreasing DO.

$10 \mu\text{mol L}^{-1}$ ) occurred in deeper anoxic waters, that is, below 130 m in April and at 160 m in June and August (Figure 2a). Nitrite concentrations were generally low ( $< 0.5 \mu\text{mol L}^{-1}$ ) throughout the water column for all sampling dates. Local  $\text{NO}_2^-$  maximum concentrations ( $\sim 0.3 \mu\text{mol L}^{-1}$ ) occurred above the oxic-anoxic interface (Figure 2b). The concentrations of  $\text{NO}_2^-$  were below detection at the anoxic depths. The distribution of  $\text{NO}_3^-$  showed a somewhat opposite distribution to that of  $\text{NH}_4^+$ . In oxygenated waters between 75 and 100 m,  $\text{NO}_3^-$  concentrations were 25–30  $\mu\text{mol L}^{-1}$ ; the concentrations decreased markedly at deeper depths, coinciding with an increase of  $\text{NO}_2^-$  above the oxic-anoxic interface (Figure 2c). Very low  $\text{NO}_3^-$  concentrations ( $< 0.2 \mu\text{mol L}^{-1}$ ) occurred in deep anoxic waters.

### 3.2. Nitrous Oxide Concentration and Isotopes

Water column  $\text{N}_2\text{O}$  concentrations were 10–29  $\text{nmol L}^{-1}$  above the oxic-anoxic interface and decreased with depth. From April to October,  $\text{N}_2\text{O}$  concentrations at oxycline depths (75–110 m) progressively increased (Figure 2d). Supersaturations of  $\text{N}_2\text{O}$  ( $\Delta\text{N}_2\text{O}$  up to 20  $\text{nmol L}^{-1}$ ) were observed at shallower oxycline depths from April to October (Figure 3a). Within the anoxic depths in April, June, and August, pronounced  $\text{N}_2\text{O}$  undersaturation ( $\Delta\text{N}_2\text{O}$  ranged from  $-7.7$  to  $-9.3 \text{ nmol L}^{-1}$ ) was observed. From August to October,  $\text{N}_2\text{O}$  concentrations at 160 m increased to near equilibrium concentration ( $\Delta\text{N}_2\text{O} = 1 \text{ nmol L}^{-1}$ ). The oxygenated and suboxic depths had variable  $\delta^{15}\text{N}_{\text{bulk-N}_2\text{O}}$  values ranging from 5‰ to 10‰ (Figure 3b) and  $\delta^{18}\text{O-N}_2\text{O}$  40‰ to 49‰ (Figure 3c). SP values were 15–25‰ and generally increased with depth and with decreasing DO (Figure 3d). The only isotope/isotopomer sample from the anoxic depths was at 160 m in August, where the values of  $\delta^{15}\text{N}_{\text{bulk-N}_2\text{O}}$ ,  $\delta^{18}\text{O-N}_2\text{O}$ , and SP were 0.4‰, 45‰, and 11‰, respectively.

### 3.3. Nitrous Oxide Production Pathways

Production of  $\text{N}_2\text{O}$  from  $\text{NH}_4^+$  oxidation occurred in the oxygenated and suboxic waters, coinciding with positive  $\Delta\text{N}_2\text{O}$  concentrations. In April, June, and August, rates of  $\text{N}_2\text{O}$  production peaked at 100–110 m (Figures 4a–4c) where in situ DO was 50–80  $\mu\text{mol L}^{-1}$ . The maximum rate of  $\text{N}_2\text{O}$  production from  $\text{NH}_4^+$  oxidation was much higher in April ( $0.35 \text{ nmol-N L}^{-1} \text{ day}^{-1}$ ) than those in June and August ( $\sim 0.05 \text{ nmol-N L}^{-1} \text{ day}^{-1}$ ).

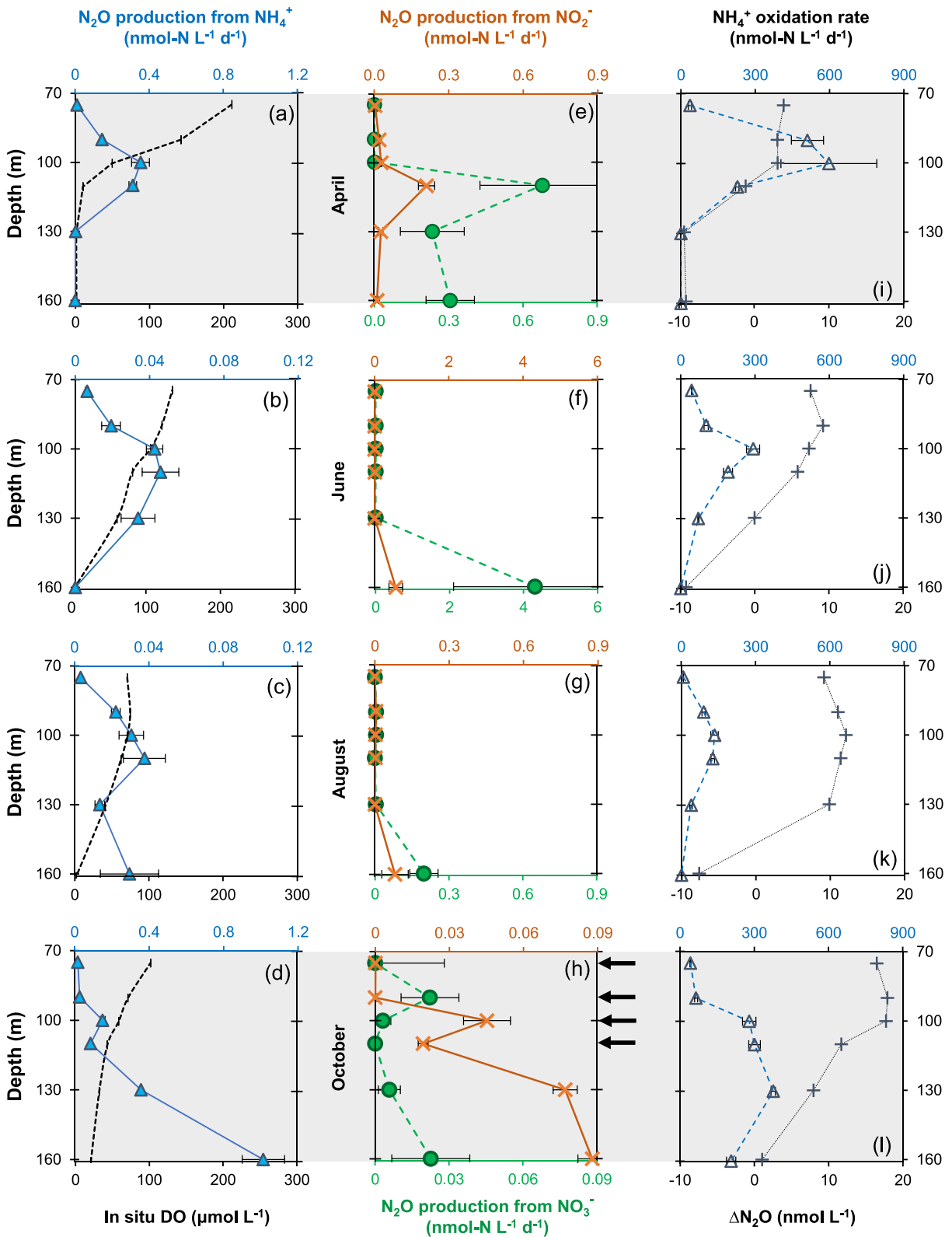


**Figure 4.** Profiles of  $N_2O$  production rates, nitrification rates, and corresponding dissolved oxygen concentrations. (a–d)  $N_2O$  production from  $NH_4^+$  oxidation (triangle) and dissolved oxygen profile (dashed line). (e–h)  $N_2O$  production from  $NO_2^-$  (cross) and  $NO_3^-$  reduction (circle). (i–l) Nitrification rate (triangle) and  $\Delta N_2O$  concentrations (plus sign) during four sampling campaigns (a, e, and i: April; b, f, and j: June; c, g, and k: August; d, h, and l: October). Arrows in (h) indicate that rate measurements were conducted under air headspace, thus having  $DO = 180\text{--}210 \mu\text{mol L}^{-1}$ , whereas the rest of the incubations were conducted under  $N_2$  headspace, having dissolved oxygen about 40% of in situ levels (see Table S1).



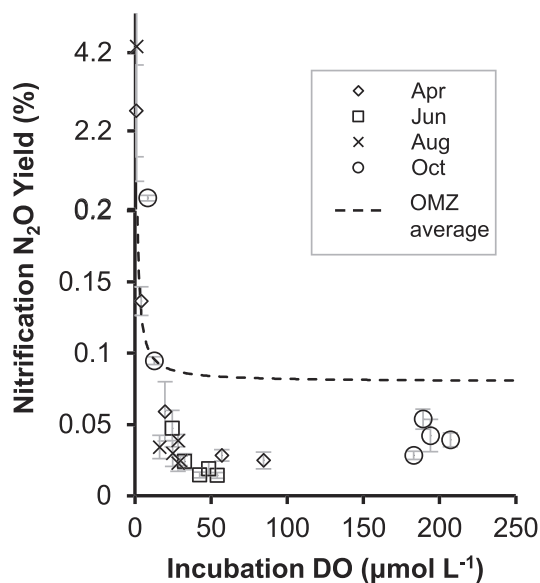


**Figure 5.**  $\text{N}_2\text{O}$  yield during  $\text{NH}_4^+$  oxidation in Saanich Inlet, measured as rate ratios of  $\text{N}_2\text{O}$  production versus  $\text{NH}_4^+$  oxidation by  $^{15}\text{N}$  incubation experiments (referred to as *rate ratio yield*) during sampling in April (diamonds), June (squares), August (crosses), and October (circles). Dashed line represents the average yield reported by Ji et al. (2018) for the eastern tropical South and North Pacific oxygen minimum zones. Note that the scale on y axis is nonlinear.

### 3.4. Nitrification and Nitrous Oxide Yield

Nitrification (measured as  $\text{NH}_4^+$  oxidation to  $\text{NO}_2^-$  plus  $\text{NO}_3^-$ ) occurred in oxygenated and suboxic zones ( $\text{DO} > 2.5 \mu\text{mol L}^{-1}$ ) from April to October. Both shallow ( $<90 \text{ m}$ ) and deep ( $160 \text{ m}$ ) layers had lower rates, while the highest rates often occurred at suboxic depths close to the oxic-anoxic interface (Figures 4i–4l). Maximum rates were  $130\text{--}600 \text{ nmol-N L}^{-1} \text{ day}^{-1}$  at in situ  $\text{DO} = 30\text{--}140 \mu\text{mol L}^{-1}$  from April to October. Nitrification was not detected at  $160 \text{ m}$  in April and June, and rates were comparably low at  $130 \text{ m}$  in April ( $0.08 \text{ nmol-N L}^{-1} \text{ day}^{-1}$ , Figure 4i) and at  $160 \text{ m}$  in August ( $0.68 \text{ nmol-N L}^{-1} \text{ day}^{-1}$ , Figure 4l). Two independent estimates of  $\text{N}_2\text{O}$  yield during nitrification are compared as follows. The rate ratio yield ranged from  $0.014$  to  $0.059\%$  at  $\text{DO} = 15\text{--}210 \mu\text{mol L}^{-1}$  during bottle incubations and increased significantly to  $4.3 \pm 3.4\%$  at  $\text{DO} < 1 \mu\text{mol L}^{-1}$  in a nonlinear fashion (Figure 5). Using nitrate concentration and  $\Delta\text{N}_2\text{O}$  data in this study and from time series observations from Torres-Beltrán et al. (2017), the regression yield was  $0.045 \pm 0.006\%$ , which is within the range of the rate ratio yield from direct measurements at  $\text{DO} > 15 \mu\text{mol L}^{-1}$  ( $0.014\text{--}0.059\%$ ).

## 4. Discussion

Saanich Inlet is a model coastal system with vertical and temporal gradients of oxygen and inorganic nitrogen that can be ideal for investigating  $\text{N}_2\text{O}$  dynamics. Incubation experiments with  $^{15}\text{N}$ -labeled substrates directly measured the rates of  $\text{N}_2\text{O}$  production via  $\text{NH}_4^+$  oxidation,

$\text{NO}_2^-$  reduction, and  $\text{NO}_3^-$  reduction under variable DO gradients. This allows for an objective assessment of the relative contributions of oxidative and reductive  $\text{N}_2\text{O}$  production pathways, as well as the regulatory effects of DO. Evidently,  $\text{NH}_4^+$  oxidation was the dominant  $\text{N}_2\text{O}$  production pathway throughout our sampling period under oxygenated conditions ( $\text{DO} > 15 \mu\text{mol L}^{-1}$ , Figure 6a). Incubation experiments demonstrating potential  $\text{N}_2\text{O}$  production rates from the oxycline to anoxic depths are important for interpreting temporal and vertical  $\Delta\text{N}_2\text{O}$  profiles. Samples with positive  $\Delta\text{N}_2\text{O}$  concentrations generally co-occurred with higher rates of  $\text{N}_2\text{O}$  production via  $\text{NH}_4^+$  oxidation than rates of  $\text{NO}_2^-$  and  $\text{NO}_3^-$  reduction (Figure 6b). Active  $\text{NO}_2^-$  and  $\text{NO}_3^-$  reduction to  $\text{N}_2\text{O}$  were mostly confined to suboxic and anoxic waters ( $\text{DO} < 15 \mu\text{mol L}^{-1}$ ). Furthermore,  $\text{N}_2\text{O}$  was undersaturated at anoxic depths, indicating net  $\text{N}_2\text{O}$  consumption as a result of complete denitrification. Both  $\text{NO}_3^-$  and  $\text{NO}_2^-$  reduction to  $\text{N}_2\text{O}$  can be regarded as partial denitrification; however, it has been shown that the two pathways were performed independently by denitrifying cells, and intracellular exchange of  $\text{NO}_2^-$  was not detected (Ji et al., 2018). Thus, rates of  $\text{NO}_3^-$  and  $\text{NO}_2^-$  reduction to  $\text{N}_2\text{O}$  were measured separately, and it is unnecessary for the two sets of rates to match. Furthermore, these potential rates were detected at depths with near depletion of  $\text{NO}_2^-$  and  $\text{NO}_3^-$  (Figures 2b and 2c); thus, addition of  $^{15}\text{N}$ -labeled  $\text{NO}_2^-$  and  $\text{NO}_3^-$  substrates could stimulate  $\text{N}_2\text{O}$  production via partial denitrification mediated by active denitrifying microbial communities (Capelle et al., 2018; Zaikova et al., 2010) capable of short-term response to inputs of electron acceptors.

As previously explained,  $^{15}\text{N}$  incubation experiments were performed under altered DO, and this had minimal effect on determining the major  $\text{N}_2\text{O}$  production pathway in the water column. Potential microbial activities in the water column were demonstrated by these measured rates, which can be comparable provided that they were conducted under similar experimental conditions (e.g., comparable rates measured from  $\text{N}_2$ -headspace vials). For example, during incubation experiments in October, the  $130$  and  $160 \text{ m}$  samples had decreased DO with respect to in situ values (Table S1), which may have stimulated  $\text{N}_2\text{O}$  production from  $\text{NH}_4^+$  oxidation. The oxycline samples ( $75\text{--}110 \text{ m}$ ) were treated with air headspace and had higher DO than in situ levels. While it is possible that  $\text{N}_2\text{O}$  production from  $\text{NH}_4^+$  oxidation was inhibited by elevated DO (see section 3.3), these October samples from  $75$  to  $110 \text{ m}$  also showed higher rates ( $0.02\text{--}0.15 \text{ nmol-N L}^{-1} \text{ day}^{-1}$ ) in comparison to August samples from the same depths, which were conducted under  $\text{N}_2$

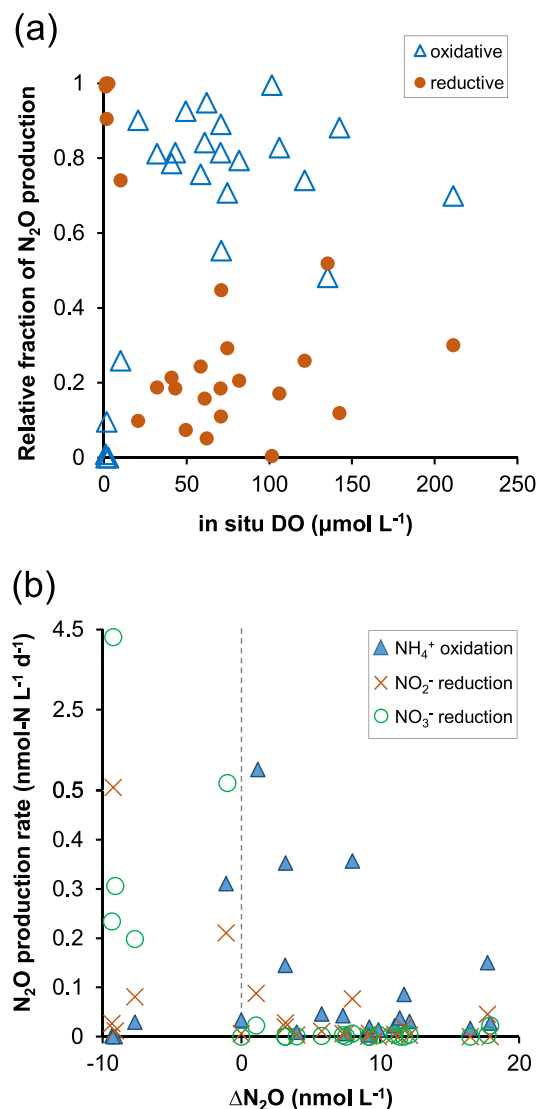


**Figure 6.** (a) The fraction of N<sub>2</sub>O production from oxidative pathway (NH<sub>4</sub><sup>+</sup> oxidation, open triangle) and reductive pathway (NO<sub>2</sub><sup>-</sup> + NO<sub>3</sub><sup>-</sup> reduction, filled circle) plotted against in situ dissolved oxygen concentration. (b) Rates of N<sub>2</sub>O production via NH<sub>4</sub><sup>+</sup> oxidation (triangle), NO<sub>2</sub><sup>-</sup> reduction (cross), and NO<sub>3</sub><sup>-</sup> reduction (circle) plotted against N<sub>2</sub>O supersaturation (ΔN<sub>2</sub>O). Dashed line marks saturated N<sub>2</sub>O concentration with respect to atmosphere. Note that the scale on y axis is nonlinear.

production pathways in situ. The fraction of N<sub>2</sub>O produced via NH<sub>4</sub><sup>+</sup> oxidation determined by <sup>15</sup>N tracer experiments was plotted against SP values from the corresponding samples (Figure 7b). Higher contributions from NH<sub>4</sub><sup>+</sup> oxidation results in SP values close to 25‰, whereas higher contribution from reductive pathways results in SP values close to 10‰. These data can be explained by a mixing model with two end members: one with SP = 25 ± 5‰ representing N<sub>2</sub>O production from NH<sub>4</sub><sup>+</sup> oxidation and the other with SP = 10 ± 5‰, respectively representing N<sub>2</sub>O production from NO<sub>2</sub><sup>-</sup> and/or NO<sub>3</sub><sup>-</sup> reduction. Additional studies are needed to test the robustness of using SP signatures to quantitatively determine the fraction of N<sub>2</sub>O produced via oxidative and reductive pathways in Saanich Inlet and elsewhere.

In all, the two independent methods, natural abundance isotopomers and <sup>15</sup>N tracer incubation experiments, delivered consistent results demonstrating that the dominant N<sub>2</sub>O production pathway in Saanich Inlet is NH<sub>4</sub><sup>+</sup> oxidation. A notable difference between Saanich Inlet and open ocean OMZs is high NH<sub>4</sub><sup>+</sup>

headspace. Production of N<sub>2</sub>O from NO<sub>2</sub><sup>-</sup>/NO<sub>3</sub><sup>-</sup> reduction could be overestimated because of lowered DO during the incubation experiments with N<sub>2</sub> headspace. Thus, the relative importance of partial denitrification to total N<sub>2</sub>O production could be overestimated, further substantiating our conclusion that NH<sub>4</sub><sup>+</sup> oxidation was the dominant N<sub>2</sub>O production pathway.

Two additional factors should be acknowledged when interpreting the rate measurements obtained from <sup>15</sup>N tracer incubations. (1) Variable in situ NH<sub>4</sub><sup>+</sup>, NO<sub>2</sub><sup>-</sup> and NO<sub>3</sub><sup>-</sup> concentrations resulted in 2–99% <sup>15</sup>N enrichment of substrates at the start of incubations. Therefore, rate measurements of N<sub>2</sub>O production from NH<sub>4</sub><sup>+</sup> oxidation (and nitrification) above 100 m depth and all of N<sub>2</sub>O production from NO<sub>2</sub><sup>-</sup> reduction and rates of NO<sub>3</sub><sup>-</sup> reduction at 160 m (see section 3.3) should reflect microbial potential at these depths. (2) Dilution of <sup>15</sup>N tracers during incubation experiments results in underestimation of N<sub>2</sub>O production rates. Variable dilution of <sup>15</sup>NO<sub>2</sub><sup>-</sup> was estimated (0–27%) using nitrification rate measurements. Dilution effects for other sets of tracer additions (<sup>15</sup>NH<sub>4</sub><sup>+</sup> and <sup>15</sup>NO<sub>3</sub><sup>-</sup>) were not estimated, and rates should be considered conservative.

The SP value of N<sub>2</sub>O is not merely an index characterizing the relative abundance of δ<sup>15</sup>N<sub>2</sub>O<sub>α</sub> over δ<sup>15</sup>N<sub>2</sub>O<sub>β</sub>; it also provides an additional, independent constraint of N<sub>2</sub>O production pathways with respect to <sup>15</sup>N incubation experiments. The SP value can also serve as a quantitative indicator for the fraction of N<sub>2</sub>O produced via oxidative and reductive pathways. Microbial N<sub>2</sub>O production via NH<sub>4</sub><sup>+</sup> oxidation and NO<sub>2</sub><sup>-</sup> and/or NO<sub>3</sub><sup>-</sup> reduction has SP values of 30 ± 5‰ and 0 ± 5‰, respectively, and these values are independent of substrate isotopic composition across a wide range of environments (Toyoda et al., 2017). During N<sub>2</sub>O production, the N<sub>2</sub>O isotopes and SP signatures follow mass conservation. The mass balance model proposed by Fujii et al. (2013) quantified the SP signature of N<sub>2</sub>O produced (SP<sub>produced</sub>) by the linear regression of the observed isotope values (SP<sub>observed</sub>) on the inverse N<sub>2</sub>O concentration (1/[N<sub>2</sub>O]<sub>measured</sub>). Saanich Inlet samples showed an SP<sub>produced</sub> value of 23 ± 0.6‰ (or 24 ± 1‰ without an outlier data point, Figure 7a), lending further support to NH<sub>4</sub><sup>+</sup> oxidation being the predominant N<sub>2</sub>O production pathway. Here, <sup>15</sup>N tracer incubation experiments and natural abundance SP values permitted a parallel view of N<sub>2</sub>O production pathways in bottle incubations in comparison to the predominant

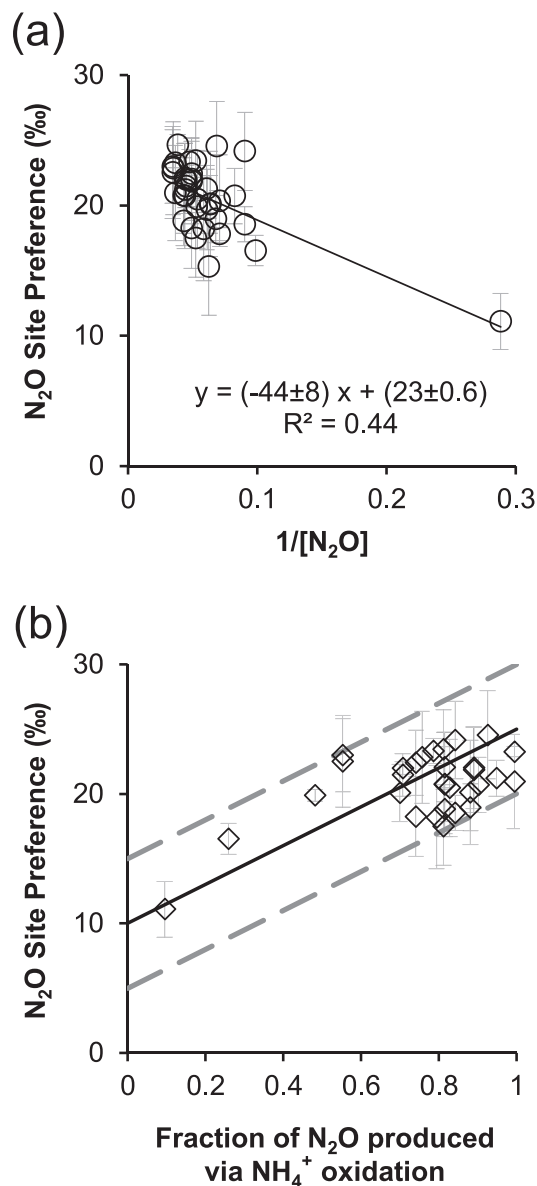


**Figure 7.** (a) Linear regression of  $N_2O$  site preference on inverse  $N_2O$  concentrations. Note: Without the outlier data point near the right edge of the plot, regression has a  $y$  intercept of  $24 \pm 1$ . (b)  $N_2O$  site preference (SP) measured in situ plotted against the fraction of  $N_2O$  production from  $NH_4^+$  oxidation measured by  $^{15}N$  incubation experiments. Solid line represents mixing between two end members, one with SP signature of 25 ‰ representing  $N_2O$  production from  $NH_4^+$  oxidation and the other with SP signature of 10 ‰ representing  $N_2O$  production from  $NO_2^-$  or  $NO_3^-$  reduction. Two dashed lines represent upper and lower SP values of  $N_2O$  when mixing between  $NH_4^+$  oxidation and  $NO_2^-$  or  $NO_3^-$  reduction having  $\pm 5\%$  variation in their respective SP signatures.

archaea (AOA) and ammonium oxidizing bacteria (AOB). Ammonia oxidizers can be found close to the oxic-anoxic interface and can utilize nanomolar oxygen level (Bristow et al., 2016; Louca et al., 2016), which can explain the detection of nitrifying activity at 130 m in April and at 160 m in August (section 3.4). In the open ocean, the ammonia oxidizing community is dominated by AOA (Horak et al., 2018), which have been shown to demonstrate higher  $N_2O$  yields than AOB (Löscher et al., 2012), and AOA is largely responsible for  $N_2O$  production (Santoro et al., 2011). In coastal zones, the relative abundance of AOB was shown to

fluxes generated by organic matter remineralization from the anoxic depth in Saanich Inlet (Bourbonnais et al., 2013). Using  $NH_4^+$  concentration profiles from this study and assuming a diffusion constant of  $1.0 \text{ m}^2 \text{ day}^{-1}$  previously estimated in Saanich Inlet 130–160 m depth (Louca et al., 2016), upward  $NH_4^+$  fluxes from the anoxic zone ranged from 0.6 to  $3.5 \text{ nmol m}^{-2} \text{ s}^{-1}$ . Such  $NH_4^+$  fluxes are similar to the Black Sea water column with sulfidic bottom water (Fuchsman et al., 2008). Similarly,  $NH_4^+$  oxidation was the dominant  $N_2O$  production pathway in the Black Sea (Westley et al., 2006).

Availability of oxygen is an important factor regulating  $N_2O$  yield during nitrification. Short-term DO changes (e.g., <3 hr) during incubation experiments can significantly change the yield (Ji et al., 2018; Löscher et al., 2012). In Saanich Inlet, the rate ratio yield increases with decreasing oxygen concentrations, particularly under suboxic conditions ( $DO < 15 \text{ } \mu\text{mol L}^{-1}$ ). Saanich Inlet samples had rate ratio yield values similar to open ocean OMZ averages at  $DO < 15 \text{ } \mu\text{mol L}^{-1}$ ; however, the yield values are generally lower than OMZ averages at  $DO > 15 \text{ } \mu\text{mol L}^{-1}$  (Figure 5). To better estimate nitrification  $N_2O$  yield using nitrate- $\Delta N_2O$  relationship, we excluded  $NO_3^-$  and  $\Delta N_2O$  data from the surface euphotic zone and deep anoxic layer and used measurements from this study and a 9-year time series data set at 40–150 m depth from a nearby station in Saanich Inlet (Torres-Beltrán et al., 2017), for two reasons: (1) Both  $NO_3^-$  and  $\Delta N_2O$  can be transported into Saanich Inlet by renewal water, which can alter the nitrate- $\Delta N_2O$  relationship especially for samples at depths below 160 m (Anderson & Devol, 1973; Capelle et al., 2018). As such,  $N_2O$  yield estimates could be altered by signals outside the inlet. (2) Both phytoplankton activity in the euphotic zone (Grundle et al., 2009) and nitrogen loss processes in the anoxic layer (Bourbonnais et al., 2013) decrease surface and bottom water  $NO_3^-$ , respectively. Using the nitrate- $\Delta N_2O$  relationship to infer regression yield across wider range of oxygen levels at various marine environments (Table 1), we found that yields in Saanich Inlet were, on average, lower than those from open-ocean OMZs influenced by coastal upwelling (e.g., the Eastern tropical South Pacific) and similar to those from oxygenated oceans (e.g., Subarctic region of Pacific and Atlantic). Furthermore, a proxy of  $N_2O$  yield during nitrification is the regression slope of  $\Delta N_2O$ -AOU relationship; compilation of  $\Delta N_2O$  versus AOU also showed Saanich Inlet to have lower ratios of  $\Delta N_2O$  versus AOU than those of open-ocean OMZs (Capelle et al., 2018; Grundle et al., 2012). Thus, we conclude that Saanich Inlet samples displayed lower  $N_2O$  yields, particularly at oxygenated conditions ( $DO > 15 \text{ } \mu\text{mol L}^{-1}$ ) than those observed in open-ocean OMZs.

As a microbial process,  $N_2O$  production from  $NH_4^+$  oxidation is mediated by two distinct microbial groups, ammonium oxidizing archaea (AOA) and ammonium oxidizing bacteria (AOB). Ammonia oxidizers can be found close to the oxic-anoxic interface and can utilize nanomolar oxygen level (Bristow et al., 2016; Louca et al., 2016), which can explain the detection of nitrifying activity at 130 m in April and at 160 m in August (section 3.4). In the open ocean, the ammonia oxidizing community is dominated by AOA (Horak et al., 2018), which have been shown to demonstrate higher  $N_2O$  yields than AOB (Löscher et al., 2012), and AOA is largely responsible for  $N_2O$  production (Santoro et al., 2011). In coastal zones, the relative abundance of AOB was shown to

**Table 1**

*Nitrification N<sub>2</sub>O Yield Indicated by Nitrate-ΔN<sub>2</sub>O Relationship (Referred to as Regression Yield) at Various Marine Environments*

Sampling location	N <sub>2</sub> O Yield (%)	O <sub>2</sub> (μmol L <sup>-1</sup> )	Depth (m)	Data source
Saanich Inlet	0.039–0.051	0–226	40–150	This study and Torres-Beltrán et al. (2017)
Eastern tropical South Pacific	0.169–0.851	20–230	5–500	Ji et al. (2019)
Mauritanian upwelling	0.130–0.257	>35	0–2930	Rees et al. (2011)
Northeast Pacific	0.08	16–342	0–600	Grundle et al. (2012)
Subarctic North Atlantic	0.057 – 0.077	210–290	20–1000	Ji and Ward (2017)

Note. See regression plots in Figures S2a and S2b, respectively.

increase with increasing DO along the oxycline (Santoro et al., 2008). In contrast, N<sub>2</sub>O yields from ammonium oxidation under suboxic conditions (DO < 15 μmol L<sup>-1</sup>) in Saanich Inlet were similar to those under open ocean suboxic conditions. This similarity may indicate that the relative importance of AOA versus AOB is more comparable between coastal and open-ocean systems when suboxic conditions persist. Further analyses of the relative abundance of AOA versus AOB from oxygenated to low oxygen conditions in Saanich Inlet will help to resolve this.

## 5. Conclusions

Saanich Inlet is characterized by temporal and vertical oxygen gradients that modulate nitrogen speciation, N<sub>2</sub>O distribution, and production pathways. The oxic-anoxic interface marks the boundary between net N<sub>2</sub>O production and consumption zones, which were indicated by N<sub>2</sub>O supersaturation and undersaturation, respectively. Above the interface, both <sup>15</sup>N tracer incubation experiments and in situ SP values confirmed that NH<sub>4</sub><sup>+</sup> oxidation is the dominant N<sub>2</sub>O production pathway, probably causing N<sub>2</sub>O supersaturation and contributing to N<sub>2</sub>O efflux to the atmosphere. We conclude that elevated N<sub>2</sub>O production from NH<sub>4</sub><sup>+</sup> oxidation following the autumn renewal event contributed to the increase of water column ΔN<sub>2</sub>O from August to October. Pronounced N<sub>2</sub>O undersaturation within the anoxic zone indicates net N<sub>2</sub>O consumption in the near absence of NO<sub>3</sub><sup>-</sup> and NO<sub>2</sub><sup>-</sup>. Such a highly reducing environment could be a net N<sub>2</sub>O sink when oxygen, NO<sub>3</sub><sup>-</sup>, and NO<sub>2</sub><sup>-</sup> are depleted, for example, removing N<sub>2</sub>O transported into the anoxic zone from the oxycline through advection/diffusion. As shown by incubation experiments, addition of NO<sub>3</sub><sup>-</sup> and NO<sub>2</sub><sup>-</sup> to anoxic samples stimulated N<sub>2</sub>O production. Conversely, reoxygenation of anoxic samples stimulated N<sub>2</sub>O production from NH<sub>4</sub><sup>+</sup> oxidation. In comparison to open ocean OMZs, Saanich Inlet has high NH<sub>4</sub><sup>+</sup> fluxes (0.6–3.5 nmol m<sup>-2</sup> s<sup>-1</sup>) from the anoxic depths that can support nitrification and associated N<sub>2</sub>O production. The dominance of NH<sub>4</sub><sup>+</sup> oxidation in N<sub>2</sub>O production in Saanich Inlet is a combination of three factors: (1) water column suboxic conditions, (2) relatively high nitrification rates (few hundred nanomole per liter per day) supported by high NH<sub>4</sub><sup>+</sup> fluxes from the anoxic layer, and (3) depletion of NO<sub>2</sub><sup>-</sup> and NO<sub>3</sub><sup>-</sup> inhibiting partial denitrification to produce N<sub>2</sub>O in suboxic and anoxic depths.

## Data Availability Statement

Readers may find all the published data in PANGAEA Repository (<https://doi.pangaea.de/10.1594/PANGAEA.912191>).

## References

- Anderson, J. J., & Devol, A. H. (1973). Deep water renewal in Saanich Inlet, an intermittently anoxic basin. *Estuarine and Coastal Marine Science*, 1(1), 1–10. [https://doi.org/10.1016/0302-3524\(73\)90052-2](https://doi.org/10.1016/0302-3524(73)90052-2)
- Bange, H. W., Arévalo-Martínez, D. L., La Paz, M. D., Farias, L., Kaiser, J., Kock, A., et al. (2019). A harmonized nitrous oxide (N<sub>2</sub>O) ocean observation network for the 21st century. *Frontiers in Marine Science*, 6. <https://doi.org/10.3389/fmars.2019.00157>
- Bange, H. W., Rapsomanikis, S., & Andreae, M. O. (1996). Nitrous oxide in coastal waters. *Global Biogeochemical Cycles*, 10(1), 197–207. <https://doi.org/10.1029/95GB03834>
- Bourbonnais, A., Lehmann, M. F., Hamme, R. C., Manning, C. C., & Juniper, S. K. (2013). Nitrate elimination and regeneration as evidenced by dissolved inorganic nitrogen isotopes in Saanich Inlet, a seasonally anoxic fjord. *Marine Chemistry*, 157, 194–207. <https://doi.org/10.1016/j.marchem.2013.09.006>
- Bristow, L. A., Dalsgaard, T., Tiano, L., Mills, D. B., Bertagnolli, A. D., Wright, J. J., et al. (2016). Ammonium and nitrite oxidation at nanomolar oxygen concentrations in oxygen minimum zone waters. *Proceedings of the National Academy of Sciences*, 113(38), 10601–10606. <https://doi.org/10.1073/pnas.1600359113>

## Acknowledgments

The authors thank Roberta Hamme and Erinn Raftery (UVic) for their generous assistance in oxygen measurements. During field sampling, Catherine Stevens and Sarah Thornton (UVic), Shirley Lyons (Victoria Capital Regional District), and Lu Guan (Ocean Networks Canada) provided valuable technical guidance. Laboratory analyses of oxygen concentrations in sample vials at the end of incubation experiments were completed with help from Amy Maas (BIOS). We thank Captain Ken Brown and crew members of the *R/V Strickland* for their professional seamanship. Financial support for this study was provided by a grant from the cluster of excellence “The Future Ocean” to D. Grundle and C. Marandino (GEOMAR), the German Research Foundation Collaborative Research Centre 754 ([www.sfb754.de](http://www.sfb754.de)), and a German Research Foundation grant to D. Grundle and C. Marandino (GR4731/2-1 and MA6297/3-1). B. Jameson was supported by the Canadian Healthy Oceans Network, University of Victoria, and NSERC CGS-M. Q. Ji was additionally supported by the Grant-In-Aid program at the Bermuda Institute of Ocean Sciences.

- Buitenhuis, E. T., Suntharalingam, P., & Le Quéré, C. (2018). Constraints on global oceanic emissions of N<sub>2</sub>O from observations and models. *Biogeosciences*, *15*(7), 2161–2175. <https://doi.org/10.5194/bg-15-2161-2018>
- Capelle, D. W., Hallam, S. J., & Tortell, P. D. (2019). Time-series CH<sub>4</sub> measurements from Saanich Inlet, BC, a seasonally anoxic fjord. *Marine Chemistry*, *215*, 103–664. <https://doi.org/10.1016/j.marchem.2019.103664>
- Capelle, D. W., Hawley, A. K., Hallam, S. J., & Tortell, P. D. (2018). A multi-year time-series of N<sub>2</sub>O dynamics in a seasonally anoxic fjord: Saanich Inlet, British Columbia. *Limnology and Oceanography*, *63*(2), 524–539. <https://doi.org/10.1002/lno.10645>
- Carpenter, J. H. (1965). The Chesapeake Bay institute technique for the Winkler dissolved oxygen method. *Limnology and Oceanography*, *10*(1), 141–143. <https://doi.org/10.4319/lo.1965.10.1.0141>
- Ciais, P., Sabine, C., Bala, G., Bopp, L., Brovkin, V., Canadell, J., et al. (2013). *Carbon and other biogeochemical cycles* (pp. 465–570). Cambridge, UK, and New York, NY.
- Codispoti, L. A. (2010). Interesting times for marine N<sub>2</sub>O. *Science*, *327*(5971), 1339–1340. <https://doi.org/10.1126/science.1184945>
- Cohen, Y. (1978). Consumption of dissolved nitrous oxide in an anoxic basin, Saanich Inlet, British Columbia. *Nature*, *272*(5650), 235–237. <https://doi.org/10.1038/272235a0>
- Coplen, T. B. (2011). Guidelines and recommended terms for expression of stable-isotope-ratio and gas-ratio measurement results. *Rapid Communications in Mass Spectrometry*, *25*(17), 2538–2560. <https://doi.org/10.1002/rcm.5129>
- Crutzen, P. J. (1970). The influence of nitrogen oxides on the atmospheric ozone content. *Quarterly Journal of the Royal Meteorological Society*, *96*(408), 320–325. <https://doi.org/10.1002/qj.49709640815>
- de Bie, M. J. M., Middelburg, J. J., Starink, M., & Laanbroek, H. J. (2002). Factors controlling nitrous oxide at the microbial community and estuarine scale. *Marine Ecology Progress Series*, *240*, 1–9. <https://doi.org/10.3354/meps240001>
- Fuchsman, C. A., Murray, J. W., & Konovalov, S. K. (2008). Concentration and natural stable isotope profiles of nitrogen species in the Black Sea. *Marine Chemistry*, *111*(1), 90–105. <https://doi.org/10.1016/j.marchem.2008.04.009>
- Fujii, A., Toyoda, S., Yoshida, O., Watanabe, S., Sasaki, K. i., & Yoshida, N. (2013). Distribution of nitrous oxide dissolved in water masses in the eastern subtropical North Pacific and its origin inferred from isotopomer analysis. *Journal of Oceanography*, *69*(2), 147–157. <https://doi.org/10.1007/s10872-012-0162-4>
- Garcia, H. E., & Gordon, L. I. (1992). Oxygen solubility in seawater: Better fitting equations. *Limnology and Oceanography*, *6*(37), 1307–1312. <https://doi.org/10.4319/lo.1992.37.6.1307>
- Gargett, A. E., Stucchi, D., & Whitney, F. (2003). Physical processes associated with high primary production in Saanich Inlet, British Columbia. *Estuarine, Coastal and Shelf Science*, *56*(5), 1141–1156. [https://doi.org/10.1016/S0272-7714\(02\)00319-0](https://doi.org/10.1016/S0272-7714(02)00319-0)
- Grundle, D. S., & Juniper, S. K. (2011). Nitrification from the lower euphotic zone to the sub-oxic waters of a highly productive British Columbia fjord. *Marine Chemistry*, *126*(1), 173–181. <https://doi.org/10.1016/j.marchem.2011.06.001>
- Grundle, D. S., Maranger, R., & Juniper, S. K. (2012). Upper water column nitrous oxide distributions in the northeast subarctic Pacific Ocean. *Atmosphere-Ocean*, *50*(4), 475–486. <https://doi.org/10.1080/07055900.2012.727779>
- Grundle, D. S., Timothy, D. A., & Varela, D. E. (2009). Variations of phytoplankton productivity and biomass over an annual cycle in Saanich Inlet, a British Columbia fjord. *Continental Shelf Research*, *29*(19), 2257–2269. <https://doi.org/10.1016/j.csr.2009.08.013>
- Hansen, H. P., & Koroleff, F. (1999). *Determination of Nutrients*. Weinheim, Germany: Wiley-VCH Verlag GmbH.
- Herlinveaux, R. H. (1962). Oceanography of Saanich Inlet in Vancouver Island, British Columbia. *Journal of the Fisheries Research Board of Canada*, *19*(1), 1–37. <https://doi.org/10.1139/f62-001>
- Holmes, R. M., Aminot, A., Kerouel, R., Hooker, B. A., & Peterson, B. J. (1999). A simple and precise method for measuring ammonium in marine and freshwater ecosystems. *Canadian Journal of Fisheries and Aquatic Sciences*, *56*, 1801–1808. <https://doi.org/10.1139/f99-128>
- Horak, R. E. A., Qin, W., Bertagnoli, A. D., Nelson, A., Heal, K. R., Han, H., et al. (2018). Relative impacts of light, temperature, and reactive oxygen on thaumarchaeal ammonia oxidation in the North Pacific Ocean. *Limnology and Oceanography*, *63*(2), 741–757. <https://doi.org/10.1002/lno.10665>
- Ji, Q., Altabet, M. A., Bange, H. W., Graco, M. I., Ma, X., Arévalo-Martínez, D. L., & Grundle, D. S. (2019). Investigating the effect of El Niño on nitrous oxide distribution in the eastern tropical South Pacific. *Biogeosciences*, *16*(9), 2079–2093. <https://doi.org/10.5194/bg-16-2079-2019>
- Ji, Q., Buitenhuis, E., Suntharalingam, P., Sarmiento, J. L., & Ward, B. B. (2018). Global nitrous oxide production determined by oxygen sensitivity of nitrification and denitrification. *Global Biogeochemical Cycles*, *32*, 1790–1802. <https://doi.org/10.1029/2018GB005887>
- Ji, Q., & Grundle, D. S. (2019). An automated, laser-based measurement system for nitrous oxide isotope and isotopomer ratios at nanomolar levels. *Rapid Communications in Mass Spectrometry*, *33*(20), 1553–1564. <https://doi.org/10.1002/rcm.8502>
- Ji, Q., & Ward, B. B. (2017). Nitrous oxide production in surface waters of the mid-latitude North Atlantic Ocean. *Journal of Geophysical Research: Oceans*, *122*(3), 2612–2621. <https://doi.org/10.1002/2016jc012467>
- Laperriere, S. M., Nidzicko, N. J., Fox, R. J., Fisher, A. W., & Santoro, A. E. (2019). Observations of variable ammonia oxidation and nitrous oxide flux in a eutrophic estuary. *Estuaries and Coasts*, *42*(1), 33–44. <https://doi.org/10.1007/s12237-018-0441-4>
- Löscher, C. R., Kock, A., Könneke, M., LaRoche, J., Bange, H. W., & Schmitz, R. A. (2012). Production of oceanic nitrous oxide by ammonia-oxidizing archaea. *Biogeosciences*, *9*(7), 2419–2429. <https://doi.org/10.5194/bg-9-2419-2012>
- Louca, S., Hawley, A. K., Katsev, S., Torres-Beltran, M., Bhatia, M. P., Kheirandish, S., et al. (2016). Integrating biogeochemistry with multiomic sequence information in a model oxygen minimum zone. *Proceedings of the National Academy of Sciences*, *113*(40), E5925–E5933. <https://doi.org/10.1073/pnas.1602897113>
- Maavara, T., Lauerwald, R., Laruelle, G. G., Akbarzadeh, Z., Bouskill, N. J., Van Cappellen, P., & Regnier, P. (2019). Nitrous oxide emissions from inland waters: Are IPCC estimates too high? *Global Change Biology*, *25*(2), 473–488. <https://doi.org/10.1111/gcb.14504>
- Manning, C. C., Hamme, R. C., & Bourbonnais, A. (2010). Impact of deep-water renewal events on fixed nitrogen loss from seasonally-anoxic Saanich Inlet. *Marine Chemistry*, *122*(1), 1–10. <https://doi.org/10.1016/j.marchem.2010.08.002>
- Rees, A. P., Brown, I. J., Clark, D. R., & Torres, R. (2011). The Lagrangian progression of nitrous oxide within filaments formed in the Mauritanian upwelling. *Geophysical Research Letters*, *38*, L21606. <https://doi.org/10.1029/2011GL049322>
- Santoro, A. E., Buchwald, C., McIlvin, M. R., & Casciotti, K. L. (2011). Isotopic signature of N<sub>2</sub>O produced by marine ammonia-oxidizing archaea. *Science*, *333*(6047), 1282–1285. <https://doi.org/10.1126/science.1208239>
- Santoro, A. E., Francis, C. A., De Sieyes, N. R., & Boehm, A. B. (2008). Shifts in the relative abundance of ammonia-oxidizing bacteria and archaea across physicochemical gradients in a subterranean estuary. *Environmental Microbiology*, *10*(4), 1068–1079. <https://doi.org/10.1111/j.1462-2920.2007.01547.x>
- Timothy, D. A., & Soon, M. Y. S. (2001). Primary production and deep-water oxygen content of two British Columbian fjords. *Marine Chemistry*, *73*(1), 37–51. [https://doi.org/10.1016/S0304-4203\(00\)00071-2](https://doi.org/10.1016/S0304-4203(00)00071-2)

- Torres-Beltrán, M., Hawley, A., Capelle, D., Bhatia, M., Durno, E., Tortell, P., & Hallam, S. J. (2016). Methanotrophic community dynamics in a seasonally anoxic fjord: Saanich Inlet, British Columbia. *Frontiers in Marine Science*, 3, 268. <https://doi.org/10.3389/fmars.2016.00268>
- Torres-Beltrán, M., Hawley, A. K., Capelle, D., Zaikova, E., Walsh, D. A., Mueller, A., et al. (2017). A compendium of geochemical information from the Saanich Inlet water column. *Scientific Data*, 4(1), 1–11. <https://doi.org/10.1038/sdata.2017.159>
- Toyoda, S., Yoshida, N., & Koba, K. (2017). Isotopocule analysis of biologically produced nitrous oxide in various environments. *Mass Spectrometry Reviews*, 36(2), 135–160. <https://doi.org/10.1002/mas.21459>
- Ward, B. B., & Kilpatrick, K. A. (1990). Relationship between substrate concentration and oxidation of ammonium and methane in a stratified water column. *Continental Shelf Research*, 10(12), 1193–1208. [https://doi.org/10.1016/0278-4343\(90\)90016-F](https://doi.org/10.1016/0278-4343(90)90016-F)
- Weigand, M. A., Foriel, J., Barnett, B., Oleynik, S., & Sigman, D. M. (2016). Updates to instrumentation and protocols for isotopic analysis of nitrate by the denitrifier method. *Rapid Communications in Mass Spectrometry*, 30(12), 1365–1383. <https://doi.org/10.1002/rcm.7570>
- Weiss, R. F., & Price, B. A. (1980). Nitrous oxide solubility in water and seawater. *Marine Chemistry*, 8(4), 347–359. [https://doi.org/10.1016/0304-4203\(80\)90024-9](https://doi.org/10.1016/0304-4203(80)90024-9)
- Westley, M. B., Yamagishi, H., Popp, B. N., & Yoshida, N. (2006). Nitrous oxide cycling in the Black Sea inferred from stable isotope and isotopomer distributions. *Deep Sea Research Part II: Topical Studies in Oceanography*, 53(17), 1802–1816. <https://doi.org/10.1016/j.dsr2.2006.03.012>
- Wilson, S. T., Bange, H. W., Arévalo-Martínez, D. L., Barnes, J., Borges, A. V., Brown, I., et al. (2018). An intercomparison of oceanic methane and nitrous oxide measurements. *Biogeosciences*, 15(19), 5891–5907. <https://doi.org/10.5194/bg-15-5891-2018>
- Yung, Y. L., Wang, W. C., & Lacis, A. A. (1976). Greenhouse effect due to atmospheric nitrous oxide. *Geophysical Research Letters*, 3(10), 619–621. <https://doi.org/10.1029/GL003i010p00619>
- Zaikova, E., Walsh, D. A., Stilwell, C. P., Mohn, W. W., Tortell, P. D., & Hallam, S. J. (2010). Microbial community dynamics in a seasonally anoxic fjord: Saanich Inlet, British Columbia. *Environmental Microbiology*, 12(1), 172–191. <https://doi.org/10.1111/j.1462-2920.2009.02058.x>
- Zakem, E. J., & Follows, M. J. (2017). A theoretical basis for a nanomolar critical oxygen concentration. *Limnology and Oceanography*, 62(2), 795–805. <https://doi.org/10.1002/lno.10461>